# Effect of High-Pressure Hot Airflow On Interlayer Adhesion Strength of 3D Printed Parts

**Huangxiang Xu**
Nanchang Hangkong University
**Jianhua Xiao** ( xjh3500021002@163.com )
Shanghai University of Engineering Science - Songjiang Campus: Shanghai University of Engineering Science
**Xiaojie Zhang**
Nanchang Hangkong University
**Xiaobo Liu**
Nanchang Hangkong University

**Research Article**

**Keywords:** 3D printing, Gas-assisted printing, Gas parameters, interlayer adhesion strength

**Posted Date:** December 15th, 2021

**DOI:** https://doi.org/10.21203/rs.3.rs-1151495/v1

# Abstract

The characteristics of FDM 3D printed parts depend largely on the process used to make them. This paper demonstrates the design of an FDM 3D printing gas-assisted molding printing head, which is used to eliminate the effect of swelling away from the mold and improve the dimensional accuracy. Meanwhile, the high-pressure hot airflow instantly heats and pressurizes the printing surface layer to enhance the interlayer adhesion strength and its mechanical properties. A stable gas lubrication layer can be formed on the inner wall of gas-assisted nozzle to smoothly deposit filaments when the gas flow ($Q_{gas}$) is set to 1.75 L/min and the gas pressure ($P_{gas}$) is set to 0.4 MPa. The interlayer adhesion strength of the printed parts is enhanced by more than 50% compared with that without gas assistance, and the volumetric shrinkage rate of the optimal group is only 0.13%. The proposed printing method can significantly improve the performance of thermoplastic parts and provide new capabilities for biomedical printing, automotive, aerospace and functional device printing in the future.


# Introduction

Additive manufacturing (AM) technology, as one of the most promising areas in the manufacturing of components [1–3], is defined as a process of joining materials to make objects based on 3D model data, usually layer upon layer, rather than a subtractive manufacturing method [4]. In recent years, it has been used in biomedicine [5, 6], the automobile industry [7, 8], and aerospace applications [9, 10]. In industrial use, the FDM method is more common than other methods because of the low cost of its printer equipment and the wide variety of consumables. In this process, the inserted filament is heated to its melting point and extruded from the nozzle to create the cross-sectional shape of the desired printed part, and each subsequent layer is fused onto the previous layer and stacked until the part is printed [11, 12]. During the printing process, the fusion of each polymer layer is due to the formation of bonds along the polymer interface. The polymer interlayer bond formation process is governed by the polymer interface healing process as is well-documented in the literature [13, 14]. The molecular chains at the polymer interface are excited by thermal energy and cross-linked with the molecular chains of adjacent filament at the contact interface. After three processes – infiltration, diffusion and bonding – the heat-driven bonding between filament is completed and the interface gradually “healed”. When the interface “healing” occurs on the interlaminar surface of an FDM print, the mechanical properties in the interfilament/layer direction will be much improved. The “healing” process of polymer interface is affected by many factors, among which the temperature and thermal diffusion time of polymer interface determine the interlayer adhesion strength of FDM printed parts [15]. This represents an opportunity to improve the ability of interlayer interfaces to “heal” by introducing process modifications independent of the native FDM process parameters to inject heat directly into the interfaces in an FDM part.

For the optimization of mechanical properties of FDM printed parts, researchers attach great importance to the optimization of FDM process inputs. For example, layer thickness [16, 17], deposition direction [18, 19], infill pattern [20, 21], printing speed [22, 23], and porosity [24, 25] affect the dimensional accuracy and overall quality of printed parts[26, 27]. Surface quality and dimensional accuracy are found to be

improved by reducing the layer thickness. In addition, the layer thickness is related to the tensile strength of the printed part [28, 29]. It was observed that the strength of the printed sample first decreases, then increases with the increase of the layer thickness due to the thermal diffusion characteristics. In addition to the optimization of process parameters, some methods have been developed to improve the mechanical properties of thermoplastic parts. O'Connor found that the use of low-pressure conditions during the printing of thermoplastic parts can increase the ultimate tensile strength of the printed part because the porosity of, and heat loss from, the printed surface can be reduced [30]. This method requires the printing set-up to be enclosed within the steel vacuum chamber and roots blower pump system to maintain low pressure in the vacuum chamber. In another approach, Lederle showed that printing in the absence of oxygen significantly improves the performance of thermoplastic parts, indicating an 8% reduction in porosity and a 42% increase in ultimate tensile strength. In general, inhibition of the oxidation process can significantly improve the effect of interlayer adhesion [31]. In addition, the influence of post-processing on the performance of printed parts is also considered. Torres used Taguchi methods to evaluate the effect of post-processing through heat treatment on part performance and found that heat treatment at low levels significantly increased the tensile strength of the PLA component while maintaining ductility and reliability [32]. Perego proposed that annealing of printed parts significantly improves the tensile strength of printed parts, because annealing can promote the change of their microstructure and the ability to crystallize, thus improving uniformity, reducing stress, and enhancing tensile strength [33]. The interaction between the printing filaments and the shape of the filaments plays an important role in the dimensional accuracy of the printed parts. For example, Lee introduced a forced-air cooling system into a 3D printer head, and the airflow speed controls the cooling of the melted filaments during printing to promote the solidification of the filaments. The study found that the dimensional accuracy of the printed model is the best when the cooling speed is 5 m/s [34]. In another approach that adds a cooling fan to the tip of the nozzle, Geng found that forced cooling of the nozzle filament can improve dimensional accuracy by affecting crystallinity and cross-linking. It was found that the maximum deviation of the printed parts decreased from +0.89/-2.38 mm under natural cooling to +0.79/-0.89 mm under forced cooling [35]. These methods require additional post-processing steps or enclosures with auxiliary equipment.

In this work, we develop a design of a gas-assisted nozzle that continuously applies a high-pressure hot airflow to the deposited surface during printing. By controlling the gas pressure ($P_{gas}$) and gas flow ($Q_{gas}$), the polymer filament is extruded via wall slip and continuously fed to the printing position on the deposited surface. When the extruded filament is in contact with the area to into which the high-pressure hot airflow is injected on the surface of the existing layer, the high-pressure hot airflow instantly heats and pressurizes the deposition surface, which reduces heat dissipation to the surrounding environment and leads to greater interlayer diffusion, thus achieving higher interlayer bonding strength. It eliminates the limitation whereby process modification is required only in the pre-manufacturing or post-processing of components.

# Experimental And Methods

In this section, the design and manufacturing details of a new gas-assisted printing head developed for FDM 3D printing are described. As shown in Fig. 1(a), the traditional 3D printing nozzle is composed of a throat, heating block, heater, temperature sensor, and brass nozzle. As shown in Fig. 1(b), the structure and size of the traditional 3D printing nozzle are adjustable. A gas inlet channel and a gas-assisted nozzle are installed at the heating block and the brass nozzle respectively. The gas inlet channel is opened at the side of the heating block for high-pressure hot airflow input. The inner wall of the gas-assisted nozzle added outside the brass nozzle adopts a streamlined curved design to ensure that the high-pressure airflow and semi-solid plastic consumables are extruded in parallel at the confluence of the nozzle. At the bottom of the gas-assisted nozzle is opened a channel with a diameter of Ø 1.2 mm for extruding molten filament and high-pressure airflow. Figs. 1(c) and (d) show the physical diagrams before and after the assembly of the gas-assisted nozzle. The pneumatic connector sits in the upper part of the nozzle, which is used to transport the high-pressure hot airflow smoothly to the inside of the gas-assisted nozzle. The gas-assisted nozzle is located below the brass nozzle, which is adopted to output and deposit high pressure hot airflow and molten polymer filament at the same time. The high-pressure hot airflow contacts the surface of the printed parts, reducing the heat dissipation to the surrounding environment and promoting the diffusion of interlayer molecules, resulting in a higher interlayer adhesion strength.

Compared with the traditional print head design, the proposed print head can optimize the disadvantages of poor dimensional accuracy and low interlayer adhesion strength: because i) a thin layer of gas lubrication is formed between the inner wall of the nozzle and the polymer filament, so that the polymer filament is extruded in the way of wall slip, eliminating the high shear and surface tension caused by the micro-size effect, and ii) gas-assisted extrusion eliminates the effect of swelling away from the mold and warpage deformation, thus improving the dimensional accuracy of the printed parts, and iii) the instantaneous heating and pressurizing effects of high-pressure airflow on the surface layer of printing parts are beneficial to interlayer macromolecular chain infiltration, diffusion, and entanglement, thus improving the interlayer adhesion and mechanical strength.

As shown in Fig. 2, the designed FDM 3D printing head is installed on the FDM 3D printer (Yinke334 single nozzle, Allcct, China) with a printing volume of 350 mm × 350 mm × 450 mm, and its movement is controlled by computer. An air compressor (750 W, 30 L, OUTSTANDING, China) controls the output end of the gas in the whole experimental device. The gas pressure ($Q_{gas}$) is controlled by a digital pneumatic regulator (AFR2000, Aceking, China), which provides deposition pressure ranging from 0 to 130 psi (896 kPa) for regulating the gas pressure output from the air compressor. Gas flow ($Q_{gas}$) by gas flow meter (LZB-4T, Tongcheng Organic Class Instrument Co., Ltd., China) control, can provide a range of 0 to 3 L/min gas flow, used to adjust the air compressor output gas flow. The gas heater (DISK, Zhaoqing HeChuang Technology Co., Ltd, China) is employed to heat the output high-pressure gas, which can provide the gas temperature in the range of 0-400°C. The printed samples were manufactured using the Yinke334 desktop 3D printer developed by Allcct, using PLA material, brass nozzle diameter is 1 mm and the gas-assisted nozzle diameter is 1.2 mm. In this study, Cura software is used to generate G code files

and command and control all process parameters. ASTM D638 is used for tensile dimensions of parts manufactured by FDM.

Gas pressure ($P_{gas}$) and gas flow rate ($Q_{gas}$), as important parameters considered in this study, are the main factors adjusted to realize the stable extrusion of filament and improve the quality of printing. To evaluate the effects of gas pressure ($P_{gas}$) and gas flow rate ($Q_{gas}$) on the interlayer adhesion strength and dimensional accuracy of printing pieces, four different gas pressures are considered: $P_{gas}$ = {0.30, 0.35, 0.40, 0.45} MPa and three different gas flows: $Q_{gas}$ = {1.50, 1.75, 2.00} L/min. As shown in Fig. 3, the experimental parts were printed in an upright fashion to measure the interlayer adhesion strength of the printed parts. The mechanical properties of parts manufactured by FDM technology depend on the selection of process parameters. To reduce the influences of other parameters, the FDM process parameters listed in Table 1 are used throughout. The nozzle temperature is kept at 210°C and the construction platform temperature is set at 50°C during each construction process. To control the same gas temperature at the nozzle and melt temperature, considering the loss of heat, the outlet temperature of the gas heater is set to 300°C, and the gas temperature at the nozzle is 210°C.

**Table 1** Print parameters

| Print parameters | Values |
|---|---|
| Layer-thickness | 0.1 mm |
| Infill density | 100% |
| Infill pattern | Rectilinear |
| Nozzle speed | 30 mm/s |
| Filament diameter | 1.75 mm |
| Default extrusion Width | 1.0 mm |
| Brim width | 1 mm |
| Deposition orientation | 45/-45° |
| Gas heater temperature | 300℃ |
| Nozzle gas temperature | 210℃ |
| Build platform temperature | 50℃ |
| gas pressure | 0.30,0.35,0.40,0.45 MPa |
| Gas flow | 1.50,1.75,2.00 L/min |

Uniaxial tensile testing was conducted according to ASTM D638 requirements. To ensure the repeatability of the results, five samples were printed on each process parameter group, the tensile test results with the highest and lowest values were eliminated, and the remaining three values were averaged and plotted. A

100-kN universal testing machine (WDW-100, Bairoe, China) with a 5-kN weighing sensor was used for tensile test at a fixed cross-head displacement rate of 1 mm/min at a temperature of 23 °C.

The change in tensile strength of printed parts is given by:

$$\theta = \frac{P_{gas} - P_0}{P_a} (1)$$

In Formula (1), $P_{gas}$ is the tensile strength of the printed part under gas-assisted condition, and $P_0$ is the tensile strength of the printed part without recourse to gas-assisted conditions.
The change in dimensional accuracy of the printed example model is given by:

$$S = \frac{D - D_{gas}}{D} (2)$$

In Formula (2), $D$ is the original size of the printed model, and $D_{gas}$ represents the actual size of the printed model.

A scanning electron microscope (SEM) (SU1510, HITACHI, Japan) was used to analyze the cross-section of the sample and to help clean the debris and burrs from the sample surface. Since the PLA printed parts are formed from non-conductive material, it is necessary to sputter an additional conductive thin layer of material on the sample surface and reduce the hardness of the vacuum applied to the sample cavity. The scanning voltage is set to 20.0 kV, the working distance is set to 15.2 mm, and the magnification is set to 50-fold.

# Results And Discussion

To stably extrude molten filament, $P_{gas}$ is an important parameter that determines the smooth deposition of molten filament and keeps $Q_{gas}$ unchanged. As shown in Fig. 4(a), when $P_{gas}$ is lower than the extrusion melt pressure ($P_{melt}$), the effect of swelling away from the mold is not eliminated, gas is compressed by extrusion of the melt at the beginning, resulting in a smaller gas flow, gas stuck in nozzle could only exit gradually, until the pressure is increased to a certain value, a break-through flow causes all the gas to be released, resulting in uneven continuous extrusion of the surface of the wire, thus forming one bamboo node after another. As shown in Fig. 4(c), when $P_{gas}$ exceeds the melt extrusion pressure ($P_{melt}$), strong airflow occupies the whole nozzle export channel, the melt is not subject to gas compression, continuous accumulation in the nozzle exit causes the melt pressure to increase to a certain value, one-time accumulation of all melt extrusion results in continuous extrusion of the surface of the filament being incomplete, thus forming one “lump” after another. As shown in Fig. 4(b), by setting $P_{gas}$ equal to the melt pressure ($P_{melt}$), the state of gas and melt is relatively stable. At this time, a continuous thin layer of lubricating gas is formed on the inner wall of the nozzle, and smooth deposition of FDM filament is realized. According to the analysis of the experimental results, when $P_{gas}$ = 0.4 MPa, a

stable gas-assisted layer is formed on the inner wall of the nozzle, and smooth extrusion and deposition of FDM wire can be realized. No extrusion swelling phenomenon occurs, and the expected result is achieved. Fig. 4(d) shows that when $P_{gas}$ = 0.4 MPa, the surface of the printed parts is the smoothest and the quality thereof is optimized. To form a stable gas-assisted layer on the inner wall of the nozzle, $Q_{gas}$ is also an important parameter that must be controlled, and $P_{gas}$ remains unchanged at 0.40 MPa at this time. As shown in Fig. 4(e), when $Q_{gas}$ < 1.75 L/min, the inner wall of the nozzle cannot form a stable gas thin layer of gas lubrication. When the melt is extruded, the high shear and surface tension caused by the micro-size effect make the effect of swelling away from the mold more obvious. This results in the uneven surface of the continuous extruded filament, thus forming one gap after another. As shown in Fig. 4(g), when $Q_{gas}$ > 1.75 L/min, the gas occupies almost the entire outlet channel and the melt diameter is compressed to less than 1 mm, resulting in uneven surface and small diameter of continuous extruded filament. As illustrated in Fig. 4(f), when $Q_{gas}$ = 1.75 L/min, a stable thin layer of gas lubrication is formed on the inner wall of the nozzle, eliminating swelling away from the mold and resulting in smooth deposition of filament. Fig. 4(h) shows that when $Q_{gas}$ = 1.75 L/min, the surface smoothness of the printed parts is maximized and the molding quality is optimal (this also matches the expected results).

As shown in Figs. 5(a), (b), and (c), at a given $Q_{gas}$, the tensile strength first increases, then decreases with the increase of $P_{gas}$, and reaches the peak value when $P_{gas}$ is 0.4 MPa. It is found that when $P_{gas}$ is less than 0.4 MPa, the surface of the extruded filament is not uniform. Although the interlayer temperature and molecular diffusion time do not change, the gap between the deposited filament increases and the relative layers adhesion area is small, resulting in a low tensile strength. As $P_{gas}$ approaches 0.4 MPa, the surface of the extruded filament is almost smooth and complete, and the sample-forming quality is improved, so the tensile strength continues to increase to its maximum value. As $P_{gas}$ begins to move away from 0.4 MPa, the gap between the deposited filament begins to increase, the relative adhesion area becomes smaller, and the phenomenon of stress concentration appears at the fracture, leading to the decrease of tensile strength and the decrease of the sample-forming quality.

As shown in Fig. 5(d), the increment of tensile strength of the printed parts with gas-assistance is compared with that without gas-assistance. The result indicates that the rate of increase in tensile strength is the highest when $Q_{gas}$ is 1.75 L/min and $P_{gas}$ is 0.4 MPa, while it is the lowest when $Q_{gas}$ is 2 L/min and $P_{gas}$ is 0.45 MPa (albeit it remains above 50% of its maximum value). The enhanced mechanical strength obtained by printing parts with gas-assisted may be a combination of several factors. Firstly, the instantaneous heating and pressurizing effects of the high-pressure hot airflow on the surface layer of printing are conducive to the interlayer macromolecular chain infiltration, diffusion and entanglement. Secondly, the decrease of porosity in gas-assisted printed parts can enhance the inter-layer adhesion. Finally, the factor that may increase the tensile strength of the printed part is the reduction of residual stress. It has been widely reported that, at standard atmospheric pressure, uneven thermal gradients and stress accumulation result from repeated heating and cooling cycles during deposition of the upper layer of print. In the case of input high-pressure hot airflow deposition, since the heat loss is

very small and the printed part is not completely cooled, the manufactured parts are unaffected by the same thermal gradient or cooling cycle. In addition, the reduction in cooling of prints printed under gas-assisted conditions can enhance the inter-layer adhesion by thermally driven molecular diffusion between layers, thus improving the tensile strength of the printed parts.

To ascertain the reasons for the improvement of mechanical properties of gas-assisted printed parts, an SEM (SU1510) is used to scan the tensile cross-section of the samples to observe the interlayer adhesion of the samples (Fig. 6). As shown in Fig. 6(a), at $Q_{gas}$ = 1.75 L/min and $P_{gas}$ = 0.30 MPa, obvious voids and cracks appear within the section. This is because $P_{gas}$ is too small. When the gas is accumulated to equal to $P_{melt}$, the diameter of the extruded filament becomes smaller when the gas is flushed out in one rapid event, and the surface of the filament is uneven, showing one bamboo node after another. There are gaps between the adjacent filament on the printing surface, leading to poor mechanical properties. As shown in Fig. 6(b), with the increase of gas pressure, when $Q_{gas}$ = 1.75 L/min and $P_{gas}$ = 0.35 MPa, the void within the section disappears, the crack is ameliorated, there are obvious brittle fracture zones, and the tensile strength is improved, which is consistent with the measured mechanical properties. As shown in Fig. 6(c), at $Q_{gas}$ = 1.75 L/min and $P_{gas}$ = 0.40 MPa, the surface of the fracture is smooth, the voids are practically eliminated, and the interlayer quality and adhesion are optimized. As shown in Fig. 6(d), at $Q_{gas}$ = 1.75 L/min and $P_{gas}$ = 0.45 MPa, cracks begin to worsen, voids expand, and defects and stress concentration are formed in the accumulation of filament. This is because $P_{gas}$ is too large. When the accumulation of $P_{melt}$ exceeds $P_{gas}$, the melt breaks out in a single event, leading to the accumulation of filament. Stress concentration ensues, resulting in poor mechanical properties.

As shown in Fig. 7, to assess the effect of the gas-assisted nozzle printing example model designed in this study, three sample models were printed under the optimal gas parameters, $Q_{gas}$ = 1.75 L/min and $P_{gas}$ = 0.4 MPa. For thin-walled parts (Figs. 7a and 7d), compared with the conditions without gas-assistance, the surface of the air-assisted printed parts is found to be smooth from the surface, and the printing track is clearly observed. From the edge, the edge of the printed parts shows no excess burring and the surface is smooth, and the fusion between layers is ideal, with almost no gap. For cuboidal parts (Figs. 7b and 7e), compared with the conditions without gas-assistance, the gas-assisted printed parts have distinct connections at each surface, without excess burr and debris, exhibiting good molding effects. For columnar parts (Figs. 7c and 7f), compared with the conditions without gas-assistance, the surface of the air-assisted printed parts fits well with the side connection, without excess burrs, and the side surface has no obvious boundary, no obvious warping and stratification, with uniform texture and good molding effects. Fig. 7(g) shows the rate of shrinkage in dimensional accuracy of the printed sample model at $Q_{gas}$ = 1.75 L/min and $P_{gas}$ = 0.4 MPa without gas-assistance. In general, compared with the non-gas-assisted condition, the shrinkage of the parts under gas-assisted condition in the three directions of length, width, and height decreases to varying degrees, with the greatest shrinkage being in the height direction. At the same time, the size error shrinkage rate in the three directions of the gas-assisted printing parts is within 2.5%, and the accuracy is relatively high. Among them, the height direction of the columnar parts is the best (the shrinkage rate therein is only 0.13%), therefore, the design

of the print head based on the combination of the proposed gas-assistance and FDM printing technique improves the dimensional accuracy and mechanical strength between layers of 3D printed parts, and promotes the application of 3D printing in medical, aerospace, automotive, and other fields.

# Conclusion

In conclusion, a novel FDM 3D printing gas-assisted nozzle is developed, which forms a thin layer of lubricating gas between the inner wall of the nozzle and the polymer filament, so that the polymer filament is extruded via wall slip. The formation of a stable gas lubrication layer can be precisely controlled by adjusting the $Q_{gas}$ and $P_{gas}$. The results show that when $Q_{gas}$ = 1.75 L/min, $P_{gas}$ = $P_{melt}$ = 0.4 MPa, the surface quality of the extruded filament is optimal, the forming quality is optimal, the mechanical properties of the printed parts are optimal, the rate of increase in tensile strength exceeds 50%, the height-direction dimensional precision shrinkage rate is optimal (with a shrinkage rate of only 0.13%). The proposed printing method also shows excellent repeatability and reliability in different printing cycles. The method is easily extended to other thermoplastics and it significantly improves the mechanical properties of the printed material. It represents the development trend of FDM 3D printing technology, and allows many potential applications in the medical, automotive, and aerospace industries.

# Declarations

Funding

This work was supported by the National Natural Science Foundation of China (NSFC) (No. 52063021). Grant Recipient: Jianhua Xiao.

Conflicts of interest

All authors certify that they have no affiliations with or involvement in any organization or entity with any financial interest or non-financial interest in the subject matter or materials discussed in this manuscript.

Availability of data and material (Not applicable)

Code availability (Not applicable)

Ethics approval

The material has not been published in whole or in part elsewhere. The paper is not currently being considered for publication elsewhere.

Consent to participate

All authors have been personally and actively involved in substantive work leading to the report, and will hold themselves jointly and individually responsible for its content.

Consent for publication

All the authors agreed to publish the manuscript as a journal article.

Authors' contributions

Huangxiang Xu: investigation; data curation; writing-original draft preparation; writing-reviewing and editing

Jianhua Xiao: funding acquisition; visualization; methodology; formal analysis

Xiaojie Zhang: conceptualization; funding acquisition

Xiaobo Liu: investigation; validation

# References


1. Tymrak BM, Kreiger M, Pearce JM (2014) Mechanical properties of components fabricated with open-source 3D printers under realistic environmental conditions. Mater Des 58:242–246. https://doi.org/10.1016/j.matdes.2014.02.038
2. Sugavaneswaran M, Arumaikkannu G (2015) Analytical and experimental investigation on elastic modulus or reinforced additive manufactured structure. Mater Des 66:29–36. https://doi.org/10.1016/j.matdes.2014.10.029
3. Melenka GW, Cheung BKO, Schofield JS, Dawson MR, Carey JP (2016) Evaluation and prediction of the tensile properties of continuous fiber-reinforced 3D printed structures. Compos Struct 153:866–875. https://doi.org/10.1016/j.compstruct.2016.07.018
4. Dizon JRC, Espera AH, Chen Q, Advincula RC (2018) Mechanical characterization of 3D-printed polymers. Addit Manuf 20:44–67. https://doi.org/10.1016/j.addma.2017.12.002
5. Cailleaux S, Sanchez-Ballester NM, Gueche YA, Bataille B, Soulairol L (2021) Fused Deposition Modeling (FDM), the new asset for the production of tailored medicines. J Control Release 330:821–841. https://doi.org/10.1016/j.jconrel.2020.10.056
6. Thomas DJ, Mohd Azmi MAB, Tehrani Z (2014) 3D additive manufacture of oral and maxillofacial surgical models for preoperative planning. Int J Adv Manuf Tech 71:1643–1654. https://doi.org/10.1007/s00170-013-5587-4
7. Prada JG, Cazon A, Carda J, Aseguinolaza A (2016) Direct digital manufacturing of an accelerator pedal for a formula student racing car. Rapid Prototyp J 22:311–321. https://doi.org/10.1108/RPJ-05-2014-0065
8. Ilardo R, Williams, Christopher B (2010) Design and manufacture of a formula SAE intake system using fused deposition modeling and fiber-reinforced composite materials. Rapid Prototyp J 16:174–179. https://doi.org/10.1108/13552541011034834

9. Zhang YJ, Moon SK (2021) The Effect of Annealing on Additive Manufactured ULTEM (TM) 9085 Mechanical Properties. Materials 14(11):2907. https://doi.org/10.3390/ma14112907
10. Choe CM, Sok SH, Ri WS, Yang WC, Kim UH (2021) Manufacture of plaster core mold for large oxygen plant components using fused deposition modeling (FDM). Int Metalcast 15(4):1275–1281. https://doi.org/10.1007/s40962-020-00549-5
11. Upcraft S, Fletcher R (2003) The rapid prototyping technologies. Assembly Autom 23(4):318–330. https://doi.org/10.1108/01445150310698634
12. Wong KV, Hernandez A (2012) A review of additive manufacturing. ISRN Mech Eng 2012:208760. https://doi.org/10.5402/2012/208760
13. de Gennes PG (1971) Reptation of a polymer chain in the presence of fixed obstacles. J Chem Phys 55:572–579. https://doi.org/10.1063/1.1675789
14. Wool RP, Yuan BL, McGarel OJ (1989) Welding of polymer interfaces. Polym Eng Sci 29(19):1340–1367. https://doi.org/10.1002/pen.760291906
15. Sun Q, Rizvi GM, Bellehumeur CT, Gu P (2008) Effect of processing conditions on the bonding quality of FDM polymer filaments. Rapid Prototyp 14(2):72–80. https://doi.org/10.1108/13552540810862028
16. Ayrilmis N, Kariz M, Kwon JH, Kuzman MK (2019) Effect of printing layer thickness on water absorption and mechanical properties of 3D-printed wood/PLA composite materials. Int J Adv Manuf Tech 102:2195–2200. https://doi.org/10.1007/s00170-019-03299-9
17. Alafaghani A, Qattawi A, Alrawi B, Guzman A (2017) Experimental optimization of fused deposition modelling processing parameters: a design-for-manufacturing approach. Procedia Manuf 10:791–803. https://doi.org/10.1016/j.promfg.2017.07.079
18. Rankouhi B, Javadpour S, Delfanian F, Letcher T (2016) Failure Analysis and Mechanical Characterization of 3D Printed ABS With Respect to Layer Thickness and Orientation. J Fail Anal Prev 16:467–481. https://doi.org/10.1007/s11668-016-0113-2
19. Carneiro OS, Silva AF, Gomes R (2015) Fused deposition modeling with polypropylene. Mater Des 83:768–776. https://doi.org/10.1016/j.matdes.2015.06.053
20. Gomez-Gras G, Jerez-Mesa R, Travieso-Rodriguez JA, Lluma-Fuentes J (2018) Fatigue performance of fused filament fabrication PLA specimens. Mater Des 140:278–285. https://doi.org/10.1016/j.matdes.2017.11.072
21. Tsouknidas A, Pantazopoulos M, Katsoulis L, Fasnakis D, Maropoulos S, Michailidis N (2016) Impact absorption capacity of 3D-printed components fabricated by fused deposition modeling. Mater Des 102:41–44. https://doi.org/10.1016/j.matdes.2016.03.154
22. Chacón JM, Caminero MA, García-Plaza E, Núñez PJ (2017) Additive manufacturing of PLA structures using fused deposition modeling: effect of process parameters on mechanical properties and their optimal selection. Mater Des 124:143–157. https://doi.org/10.1016/j.matdes.2017.03.065
23. Khosravani MR, Reinicke T (2020) Effects of raster layup and printing speed on strength of 3D-printed structural components. Procedia Struct Integr 28:720–725.

https://doi.org/10.1016/j.prostr.2020.10.083

24. Tronvoll SA, Welo T, Elverum CW (2018) The effects of voids on structural properties of fused deposition modelled parts: a probabilistic approach. Int J Adv Manuf Tech 97:3607–3618. https://doi.org/10.1007/s00170-018-2148-x
25. Guessasma S, Belhabib S, Nouri H (2019) Understanding the microstructural role of bio-sourced 3D printed structures on the tensile performance. Polym Test 77:105924. https://doi.org/10.1016/j.polymertesting.2019.105924
26. Zhang HP, Wang JH, Liu YL, Zhang XS, Zhao ZY (2022) Effect of processing parameters on the printing quality of 3D printed composite cement-based materials. Mater lett 308:131271. https://doi.org/10.1016/j.matlet.2021.131271
27. Sood AK, Ohdar RK, Mahapatra SS (2009) Improving dimensional accuracy of fused deposition modelling processed part using grey Taguchi method. Mater Des 30(10):4243–4252. https://doi.org/10.1016/j.matdes.2009.04.030
28. Lanzotti A, Grasso M, Staiano G, Martorelli M (2015) The impact of process parameters on mechanical properties of parts fabricated in PLA with an open-source 3-D printer. Rapid Prototyp 21(5):604–617. https://doi.org/10.1108/RPJ-09-2014-0135
29. Rodríguez JF, Thomas JP, Renaud JE (2003) Mechanical behavior of acrylonitrile butadiene styrene fused deposition materials modelling. Rapid Prototyp J 9(4):219–230. https://doi.org/10.1108/13552540310489604
30. O'Connor HJ, Dowling DP (2018) Evaluation of the influence of low pressure additive manufacturing processing conditions on printed polymer parts. Addit Manuf 21:404–412. https://doi.org/10.1016/j.addma.2018.04.007
31. Lederle F, Meyer F, Brunotte G-P, Kaldun C, Hu¨bner EG (2016) Improved mechanical properties of 3D-printed parts by fused deposition modeling processed under the exclusion of oxygen. Prog Addit Manuf 1:3–7. https://doi.org/10.1007/s40964-016-0010-y
32. Torres J, Cotelo J, Karl J, Gordon AP (2015) Mechanical property optimization of FDM PLA in shear with multiple objectives. Miner Metals Mater Soc 67(5):1183–1193. https://doi.org/10.1007/s11837-015-1367-y
33. Lee C-Y, Liu C-Y (2019) The influence of forced-air cooling on a 3D printed PLA part manufactured by fused filament fabrication. Addit Manuf 25:196–203. https://doi.org/10.1016/j.addma.2018.11.012
34. Geng P, Zhao J, Wu WZ, Wang YL, Wang BF, Wang SB, Li GW (2018) Effect of thermal processing and heat treatment condition on 3D printing PPS properties. Ploymers 10(8):875. https://doi.org/10.3390/polym10080875
35. 35. Geng P, Zhao J, Wu WZ, Wang YL, Wang BF, Wang SB, Li GW (2018) Effect of thermal processing and heat treatment condition on 3D printing PPS properties. Ploymers 10(8):875. https://doi.org/10.3390/polym10080875.

# Figures

## Figure 1

Nozzle cross-section and physical drawing (a) traditional 3D printing nozzle (b) gas-assisted nozzle design (c) gas-assisted nozzle expansion diagram (d) gas-assisted nozzle assembly diagram.

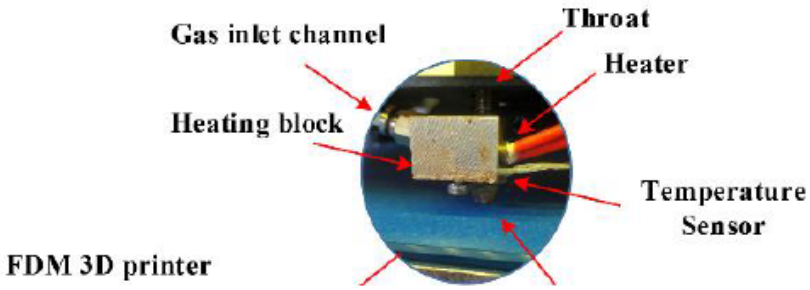


## Figure 2

Gas-assisted printing experimental device.

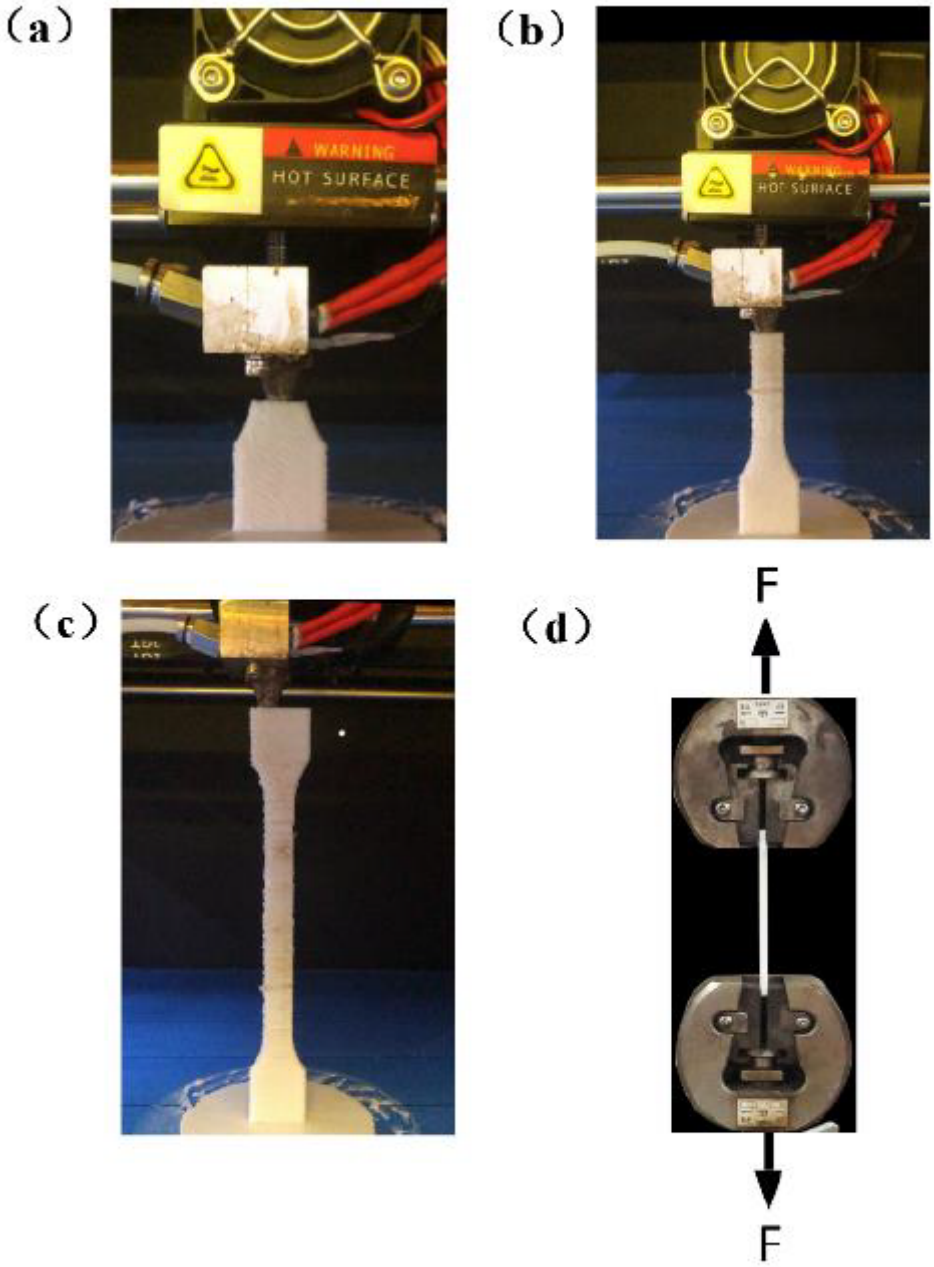


## Figure 3

Printing process and drawing diagram of specimen in upright mode.

## Figure 4

Filament extrusion and tensile specimen models with different Pgas and Qgas values.

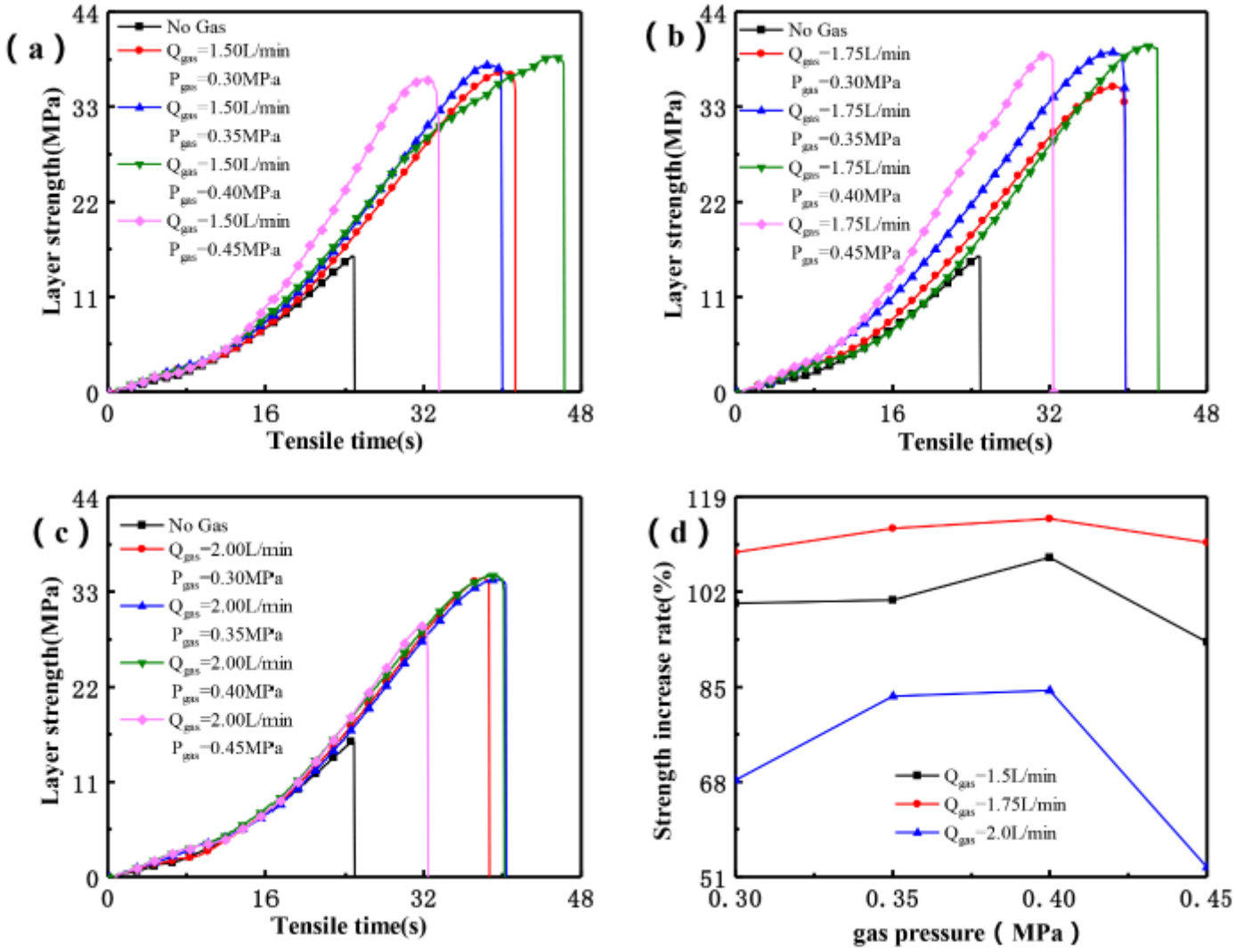


## Figure 5

Layer strength curve under different gas parameters.

## Figure 6

Fracture SEM and fracture surface morphology of 3D printed tensile parts with different gas parameters (a) Qgas = 1.75 L/min, Pgas = 0.30 MPa. (b) Qgas = 1.75 L/min, Pgas = 0.35 MPa. (c) Qgas = 1.75 L/min, Pgas = 0.40 MPa. (d) Qgas = 1.75 L/min, Pgas = 0.45 MPa.

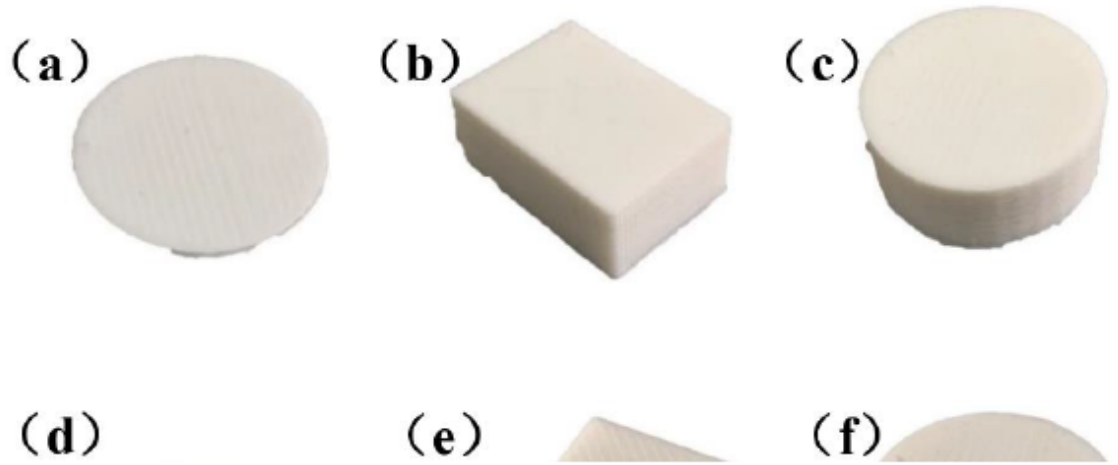


**Figure 7**

Print sample models and size shrinkage with and without gas-assisted (a) (b) (c) Qgas = 1.75 L/min, Pgas = 0.40 MPa (d) (e) (f) Non-gas-assisted (g) Comparison of dimensional shrinkages.